Electrochimica Acta 173 (2015) 665–671

Contents lists available at ScienceDirect

Electrochimica Acta

journal homepage: www.elsevier.com/locate/electacta

Investigation of TiO_2 nanotubes/nanoparticles stacking sequences to improve power conversion efficiency of dye-sensitized solar cells

Md Ashraf Hossain [a], Jieun Park [b], Ji Young Ahn [a], Chansu Park [c], Yangdo Kim [c], Soo Hyung Kim [a,d,*], Dongyun Lee [a,d,*]

[a] Department of Nano Fusion Technology, Pusan National University, Busan 609-735, Republic of Korea
[b] Department of Cogno-Mechatronics Engineering, Pusan National University, Busan 609-735, Republic of Korea
[c] School of Materials Science and Engineering, Pusan National University, Busan 609-735, Republic of Korea
[d] Deprtment of Nano Energy Engineering, Pusan National University, Busan 609-735, Republic of Korea

ARTICLE INFO

Article history:
Received 31 March 2015
Received in revised form 14 May 2015
Accepted 24 May 2015
Available online 27 May 2015

Keywords:
Dye-sensitized solar cell
TiO_2 nanotubes
Two-step anodization
Light-scattering layer

ABSTRACT

In this study, dye-sensitized solar cells (DSSCs) were fabricated using a hybrid photoanode with freestanding TiO_2 nanotube (TN) membranes and TiO_2 nanoparticles (TPs). To form the hybrid structures, up to 20 layers of TPs were screen-printed on to fluorine-doped tin oxide (FTO) glass, and the TNs, which were grown separately, were placed on top of the TPs. To investigate the effects of TNs on the energy conversion efficiency of these cells, TNs were placed on and sandwiched between TPs. Vertically oriented and smooth TN surfaces were obtained using a two-step anodization process. To obtain crystallized TNs, heat treatment was performed and anatase crystal structure was confirmed with XRD. For the anodized-TN-based solar cells, incident light was scattered by the three-dimensional topography at the bottom of the highly ordered TNs. This effect increased the optical path length in the photoanode, which allowed more light to be recycled by the dye molecules for additional photocurrent generation. This process also yielded a significantly higher power conversion efficiency (7.0%) than other geometries of photoanodes, which was further increased to 7.5% and charge transfer resistance decreased 14.5 Ω to 5.51 Ω when the TNs were sandwiched between the TPs, which was analyzed by EIS simulation.

1. Introduction

In 1991, dye-sensitized solar cells (DSSCs) with a power conversion efficiency (PCE) of 7.12% were first reported by O'Regan and Gratzel [1]. Many subsequent studies have been conducted to improve the PCE of DSSCs, and recently, J. Burschka et al. [2] reported a perovskite-sensitized solar cell with 14.14% efficiency, which was achieved by controlling the morphology of the perovskite layer. Conversely, to date, the highest reported and certified PCE of a DSSC module based on a typical ruthenium complex, such as N3 or N719 dyes, with nanoparticulate TiO2 is about 11.9% [3]. Currently, to improve the PCE of solar cells, many studies have been conducted to investigate several different techniques, including the development of dyes, increasing the anode's surface area, and changing the anode's charge-transfer medium. Among these studies, many have been conducted to increase both the surface area and charge transfer rate, for which various types of nanostructures, including nanorods, nanowires, and nanotubes, have been tested [4–5]. Screen-printed nanoparticulate TiO2 on fluorine-doped tin oxide (FTO) glass with a monolayer of dye molecules is a typical anodic electrode. However, TiO_2 nanoparticles (TPs) form random networks and numerous grain boundaries that may reduce electron mobility, and thus, slow the transport of excited electrons; these issues reduce cell conversion efficiency [6].

Compared to TPs, self-organized and vertically aligned TiO_2 nanotubes (TNs) could provide other advantages in addition to their large surface area; TNs may also reduce the probability of recombination for electron-hole pairs and provide direct conducting pathways for electrons [7]. Based on typical methodologies, TNs have been fabricated through the electrochemical anodization of Ti foil by optimizing the electrolyte concentration, the applied anodization voltage, and the anodization time [8–11]. For the light-absorbing and electron-generating media in DSSCs, TNs have been fabricated with various methods to enlarge their surface area and thereby improve the solar cell efficiency. Researchers have reported various methods to achieve this, including making tubes with smaller diameters (usually at a low voltage) [12–14], altering the tube surface (both the inside and outside walls) through the

* Corresponding authors.
E-mail addresses: sookim@pusan.ac.kr (S.H. Kim), dlee@pusan.ac.kr (D. Lee).

http://dx.doi.org/10.1016/j.electacta.2015.05.141
0013-4686/

hydrolysis of TiCl4 (with a particle size of approximately 3 nm) [15–16], and constructing mixed architecture by filling the tubes with nanoparticles to utilize the tubes' hollow spaces [17–21].

DSSCs in which the photoanode is composed of TNs grown on Ti foil require backside illumination, which may cause the reflection and absorption of light by the counter electrode and electrolyte [22–23]. To resolve this drawback, Grimes et al. [24] fabricated a transparent TN-based photoanode through the anodization of a Ti thin-film sputtered on FTO conductive glass, but this procedure was complex, costly, and required both the special treatment of the metal layer in contact with the electrolyte surface [23] and strict processing controls [25]. In addition, it has been reported that increasing the TiO_2 film thickness leads to poor adhesion to the substrate [26–28]. Therefore, detaching TNs from the Ti substrate and attaching them to the FTO glass is another approach for preparing photoanodes for front side illuminated DSSCs. Chen and Xu [29] developed a low-potential anodization process to detach a large area of freestanding TNs and transfer them onto FTO glass. In addition, complex hierarchical nanostructures with stacked nanotubes and nanoparticles have been used to combine the properties of nanotubes and nanoparticles [30–33]. However, improving the design of photoanodes to increase the PCE and, at the same time, lower costs remains a formidable challenge because many hybrid structures do not simultaneously exhibit a highlight-harvesting efficiency, long photoelectron lifetime, desirable electron extraction, and facile operation. To avoid these issues in the present study, we combined the improved light-harvesting efficiency of front-illuminated geometries, the unidirectional photoelectron transport when using nanotubes, and the desirable electron extraction of composite structures for creating hybrid photoanodes. Furthermore, we investigated the role of the TNs in the complex hierarchical structures by altering the positioning of the tubes.

For a systematic analysis of how hybrid structures could improve the PCE of solar cells, different hybrid structures were fabricated by changing the stacking sequence of the TNs and TPs while maintaining a photoanode thickness of approximately 25 μm [34]. We also detached and transferred TNs onto FTO glass and then screen-printed TPs onto the TNs to form a layer-by-layer photoanode. To avoid other adverse side effects resulting from the shape of the TNs, we synthesized highly ordered and vertically aligned TNs on pure Ti sheets through a two-step anodization process at room temperature, and we then detached the TNs from the Ti sheet to transfer them.

2. Experimental Procedure

2.1. Sample Preparation

TNs were fabricated through a two-step anodization process with Ti foil (20 ×20 mm, 0.25-mm thick,99.9% pure, Sigma Aldrich) [31]. For the anodization process, the cleaned Ti foil was immersed in the electrolyte solution at a constant depth, with a Pt mesh acting as the counter electrode. The first anodization was conducted at 50 V for 3 h with an ethylene glycol solution (EG, 99.8% anhydrous, Sigma Aldrich) containing of NH4F (0.3 wt.%) and H_2O (2vol.%). An initial ramp rate of 0.1 V/s was used. The nanotubes that initially formed were then removed with ultrasonication, which created hexagonal patterns on the surface of the Ti foil that served as guides for forming uniform TNs. To produce well-aligned TNs, a second anodization was then performed under the same conditions for 2 h. After the anodization processes, the TNs were cleaned with ethanol in a low-agitation ultrasonic bath. For crystallization, the TNs formed on the Ti foil by the second anodization process were annealed at 450°C for 1 h. The annealed Ti foil with TNs was anodized again in the same electrolyte solution for 3 h at a relatively low potential (12 V) to form a thin, amorphous, TiO_2 layer, which helps when detaching the TNs from the Ti foil. After being rinsed in ethanol, the Ti foil was then immersed in a 10% H_2O_2 solution for 6 h to dissolve the amorphous TiO_2 layer. Consequently, the TNs formed through the two-step anodization process were separated from the substrate to form a freestanding TN membrane that was transferred to a Petri dish containing isopropyl alcohol (IPA). To transfer the TN membrane, the Ti foil was tilted and the membrane gently slid into the Petri dish. The nanotube transfer was conducted in IPA instead of air to minimize both the surface tension and potential damage to the membrane. This procedure also avoided damage that could result from any mechanical load, such as tweezers, on the membrane. The transferred TNs were then annealed again at 500°C for 2 h in the ambient atmosphere.

A 1.5×1.5cm FTO glass substrate with a sheet resistance of approximately 7Ω/Sq was successively cleaned in an ultrasonic bath with acetone, ethanol, and de-ionized water for 10 min per solvent and dried with a flow of N_2. The FTO glass was then immersed in a solution of $TiOCl_2$ for 30 min at 70°C [35] to coat the glass with an adhesion layer of TPs. The coated FTO was then annealed at 350°C and 500°C for 30 min to form a buffer layer of anatase TPs, which acts as both an adhesion layer for the additional TP layers and inhibiter of hole-electron pair recombination between the FTO glass and electrolyte. A TP paste (Ti-Nanoxide T/SP paste, Solaronix) was screen-printed onto the FTO substrates, the TNs were transferred on top of them, and then the substrate was gently pressed with slide glass to attach the TN membrane to the TP layer. After being dried in air, the TN/TP films were sintered in two steps; the films were first annealed for 10 min at 350°C and then annealed for an additional 30 min at 500°C [35]. To increase the surface area, all sintered TN/TP photoanodes were re-treated with $TiOCl_2$ and annealed. The films were then immersed in a dye solution (0.3 mM of N719 in a 1:1 mixture of acetonitrile and tert-butanol) at room temperature for 24 h. The TN/TP films were sandwiched together between a platinized FTO counter electrode and the FTO substrate with a hot-melt spacer (60-μm thick, Solaronix). To create the counter electrode, an FTO glass substrate was coated with a thin layer of Pt into which a 0.4-mm-diameter hole was drilled. Subsequently, 5 mM of H2PtCl6 in ethanol was spin-coated onto the Pt-coated FTO glass, which was then annealed at 380°C for 30 min. The electrolyte (Iodolyte AN-50, Solaronix, Switzerland) was injected into the cell through the drilled hole on the backside of the Pt-coated counter electrode. Five different photoanodes with various TN and TP stacking sequences were prepared to investigate the effect of TNs on the PCE of the DSSCs (the results, average values out of six samples, will be discussed in Table 1 and Fig. 3). For comparison, we prepared cells with only 20 layers of TPs, which is almost the same thickness of TN/TP hybrid cells (discussed in the Supporting Information). In addition, to measure the amount of dye adsorbed by the photoanodes, the dye on the photoanodes was desorbed with a 1:1 mixture of 0.1 M NaOH and ethanol. The concentration of the desorbed dye was then measured with UV-Vis absorption spectroscopy and calculated using the Beer–Lambert Law which is explained in the Supporting Information [36].

2.2. Characterization

The morphology and crystal structure of the TNs were characterized with scanning electron microscopy (SEM, Hatachi-S4700, 15 kV) and X-ray diffractometry (XRD, Empyrean, PANalytical), respectively. The current density-voltage curves of the DSSCs were measured under simulated AM 1.5-G illumination, with an irradiated area of 0.16cm^2. Electrochemical impedance spectroscopy (EIS) was performed with a potentiostat (IVIUM) under the

Table 1
The photovoltaic characterization of the DSSCs fabricated with different photoanodes[a].

Type	Sample	J_{sc}(mA·cm^{-2})	V_{oc}(V)	FF	PCE(%)	M_{DA} ($\times10^{-7}$mol·cm^{-2})
Type A	FTO/2L TPs/TNs	9.95	0.65	0.67	4.16±0.16	1.48
Type B	FTO/5L TPs/TNs	12.04	0.63	0.66	4.89±0.15	2.00
Type C	FTO/7L TPs/TNs	17.39	0.63	0.66	7.08±0.14	2.16
Type D	FTO/2L TPs/TNs/5L TPs	15.59	0.64	0.66	6.51±0.11	2.22
Type E	FTO/5L TPs/TNs/2L TPs	18.32	0.63	0.68	7.47±0.30	2.19

[a] J_{sc} = short-circuit current density, V_{oc} = open-circuit voltage, FF = fill factor, PCE = power conversion efficiency, M_{DA} = concentration of dye adsorbed.

AM 1.5 illumination. The reflectance of the photoanodes was collected over 400 to 800 nm with UV-Vis absorption spectroscopy (Thermo Fisher Scientific-EV0300PC).

3. Results and Discussion

As discussed in Section 2, the TNs were directly grown on Ti foil. The initial TNs obtained after the first anodization in the NH4F/H_2O/ethylene glycol electrolyte solution were irregularly shaped, and fragile debris was observed on the surface of the TNs with SEM (Fig. 1(a)). It was difficult to obtain a smooth surface using only the initial anodization, and the TN membrane was easily cracked and delaminated during the ultrasonic cleaning process. Furthermore, we presume that the irregular microstructures observed in the initial TNs would affect electron transport to the electrode, as well as retard the infiltration of dye and electrolyte solutions into the nanotubes [15,37]. To circumvent this issue, many researchers have reported successfully obtaining well-aligned self-organized nanotubes, which were achieved with a two-step anodization process [10,38–39]. For uniform and vertically upright structures, the initial TNs were intentionally removed through ultrasonication, which left behind hexagonal patterns on the surface of the Ti foil (Fig. 1(a) inset). The foil was then anodized again (i.e., the second anodization) to yield uniform TNs with smooth surfaces (Fig. 1(b)). We then detached the membrane to transfer the TNs onto the FTO glass to create photovoltaic cells. Even though the bottom of the freestanding membrane was capped (Fig. 1(c)), the arrays of TNs in the membrane were preserved on the bottom. From the cross-sectional view of the TN arrays (Fig. 1(d)), the thickness of the membrane was approximately 16 μm, and it confirmed that well-aligned vertically straight TNs were obtained. The XRD patterns of the anodized TN membrane were used to characterize its crystal structure. As shown in Fig. 2(a), no distinctive TiO_2 peaks are present for the as-prepared TN membranes because the membranes are mostly amorphous structures. After being annealed at 450°C for 1 h, the diffraction

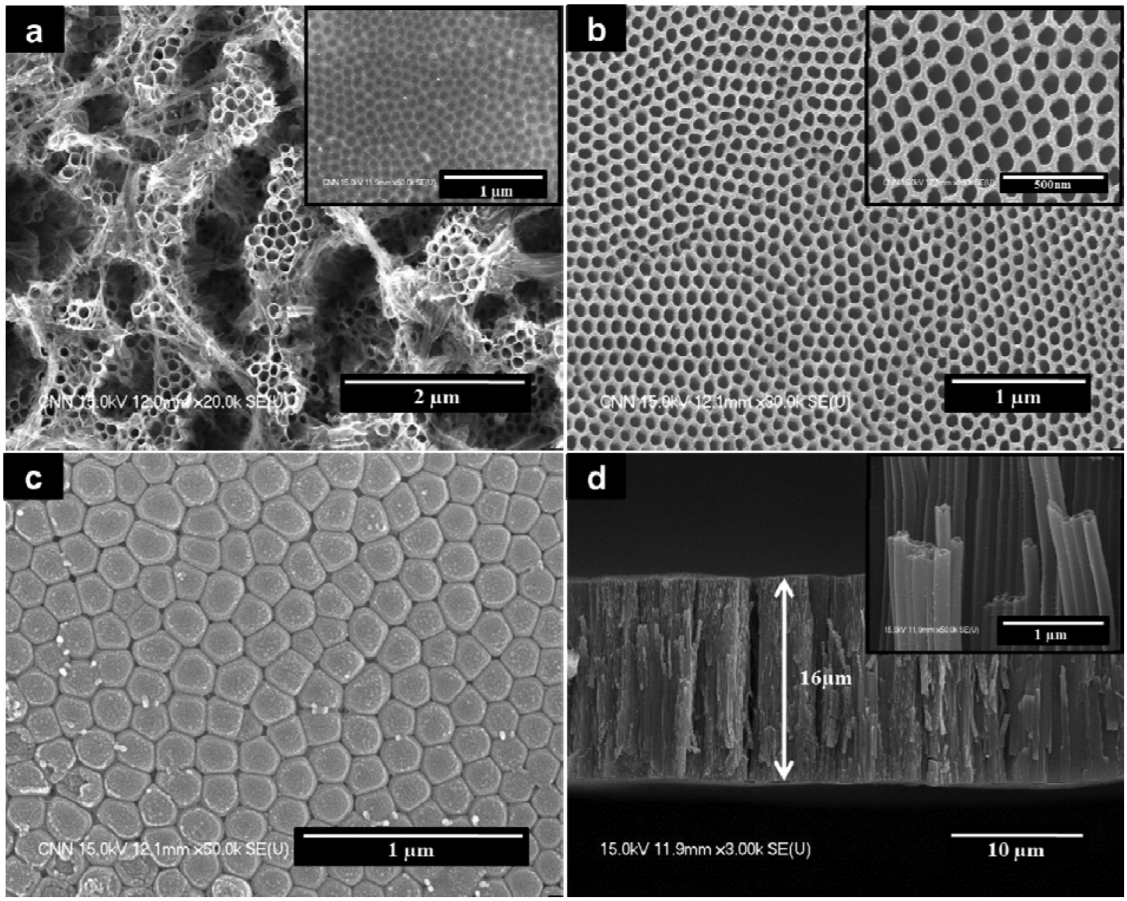

Fig. 1. SEM images of the TNs. Plane-views after the (a) first anodization for 3 h and (b) second anodization for 2 h. (c) Plane-view of the bottom of film after the second anodization. (d)A side-view of the film in (c). The inset in (a) is the corresponding view of the substrate after removing the nanotube layer with ultrasonication. The insets in (b) and (d) are magnified micrographs of the freestanding TNs shown in (b) and (d), respectively.

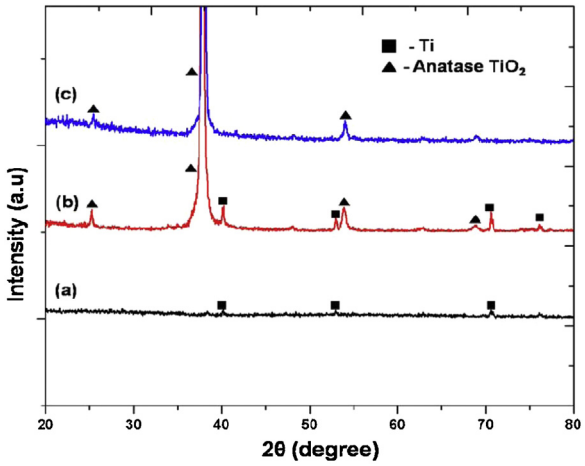

Fig. 2. XRD patterns of (a) as-prepared TNs on the Ti substrate, (b) TNs annealed on the Ti substrate at 450°C for 1 h in air, and (c) freestanding TNs annealed at 500°C for 2 h in air.

peaks corresponding to TiO_2 are clear, as shown in Fig. 2(b). For the freestanding TNs (Fig. 2(c)), the diffraction peaks of the Ti substrate have disappeared, and all of the diffraction peaks present were attributed to the anatase TiO_2 phase.

Five different light-absorbing photoanodes with various TN and TP stacking sequences were fabricated on FTO glass, and were denoted as types A, B, C, D, and E; additional information about the photoanodes fabricated with only TPs is presented in the Supporting Information. These photoanodes with various TN and TP stacking sequences and without TNs were carefully investigated to understand the role of TNs in photoanodes. In samples A, B, and C, TNs were positioned on TP layers, while TNs were sandwiched between TP layers in samples D and E. Schematics showing the layer-by-layer structures of the five photoanodes are shown in Fig. 3. To fabricate these stacked structures, the detached and brittle TNs were vertically aligned (as shown in Fig. 3) during all subsequent processes (i.e., the detaching, transferring, and annealing processes). By taking special care taken during these processes, we successfully placed the TPs on the open tops of the TNs to construct the FTO/TP/TN stacks. A photograph of the cell containing the E-type photoanode (with TNs between TPs) is shown in Fig. 4(a). A cross-sectional SEM image of the E-type photoanode and a schematic of the cross-sectional view of the cell containing the E-type photoanode are presented in Figs. 4(b) and (c), respectively. In Fig. 4(b), we can clearly see the distinct layer of vertically aligned TNs and the uniform TP layers on both sides.

The photocurrent density-voltage (*J-V*) characteristics of the DSSCs fabricated from the various photoanode structures were measured under AM 1.5 solar conditions with an intensity of 100 mW/cm^2. The curves are shown in Fig. 5, and the details of the *J-V* curves, such as the short-circuit current density (J_{sc}), open-circuit voltage (V_{oc}), fill factor (FF), PCE, and dye contents, are summarized in Table 1.The PCE of the cell fabricated with the A-type photoanode on basic FTO glass (FTO glass coated with two layers of TPs) is 4.2%. By increasing the number of TP layers on the FTO glass, the PCE increases from 4.9% for type B (five layers) to 7.0% for type C (seven layers). Based on these results, and as expected, the PCE appears to be mainly governed by the total thickness of the photoanode. A thicker layer could create a higher volume of pores into which more dye molecules could be loaded, which would thereby increase the J_{sc} in the energy-transferring medium (about 10 to 17 mA/cm^2) because of the increased generation and collection of light-generated carriers.

The PCE of the cells with no TNs in their photoelectrode are listed in Table S1, with the PCE ranging from 3.6% (2 layers of TPs, best result) to 6.4% (20 layers, best result), which is approximately 25-μm thick. Therefore, with the number of TP layers increasing by a factor of 10, the PCE is increased by less than a factor of 2. As shown in Table 1, with approximately the same thickness (about 25 μm) as that of the TP stacks, the average PCE of the C-type TP/TN hybrid structure is 7.0%, which is 9% higher than the best value of the TP-only stack. Interestingly, for TP/TN hybrid structures of the same thickness but with different stacking sequences, i.e., types C, D, and E, we obtained different results. Even though these cells have absorbing layers of equal thickness and nearly equal concentrations of adsorbed dye, as shown by the M_{DA} values listed in Table 1 (seethe Supplementary Information for further details), the PCE of the D-type cell is approximately 20% lower than that of the E-type cell, which has the best PCE of all the photoanodes tested. The PCE of the E-type cell, which has a layer of TNs placed on top of five layers of TPs and under two layers of TPs, is about 7.5%. Presumably, the enhanced PCE of the E-type cell results from the increased dwell time of the incident photons in the photoanode after the photons pass through the anode FTO glass and are reflected onto the bottom of the TNs. Furthermore, some of the photons absorbed by the dye molecules in the TNs create electrons. In addition, electrons created in the TN and TP layers are easily transferred through the TNs because they provide direct conducting pathways for these electrons. As previously reported [40], anodized TNs exhibit improved light-harvesting abilities because of the enhanced light scattering, which extends the dwell time to create more electrons in the adsorption layer. This scattered light can be recycled in the anode of DSSCs, which improves the PCE. Furthermore, compared to the TP-only-type

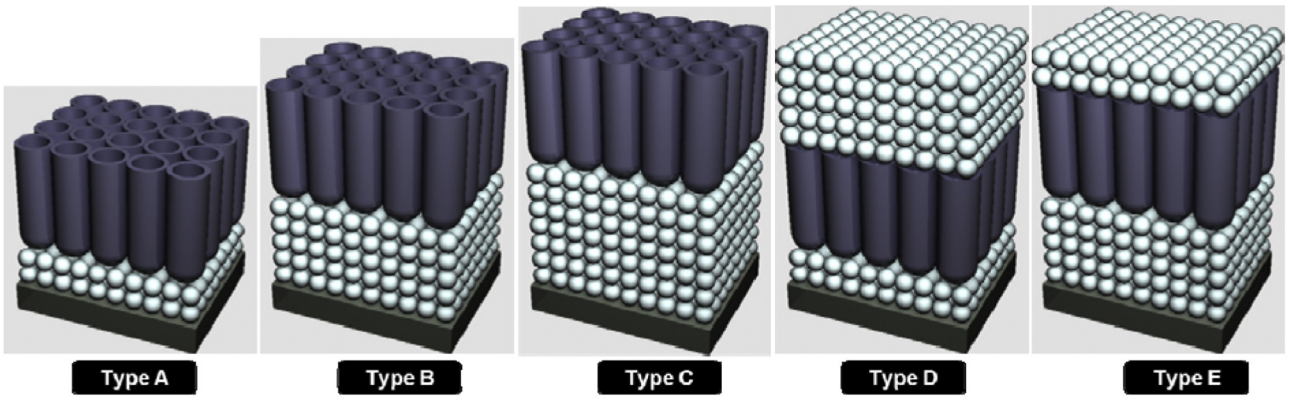

Fig. 3. Schematics of the TP/TN stacking sequences of the photoanodes tested in this study.

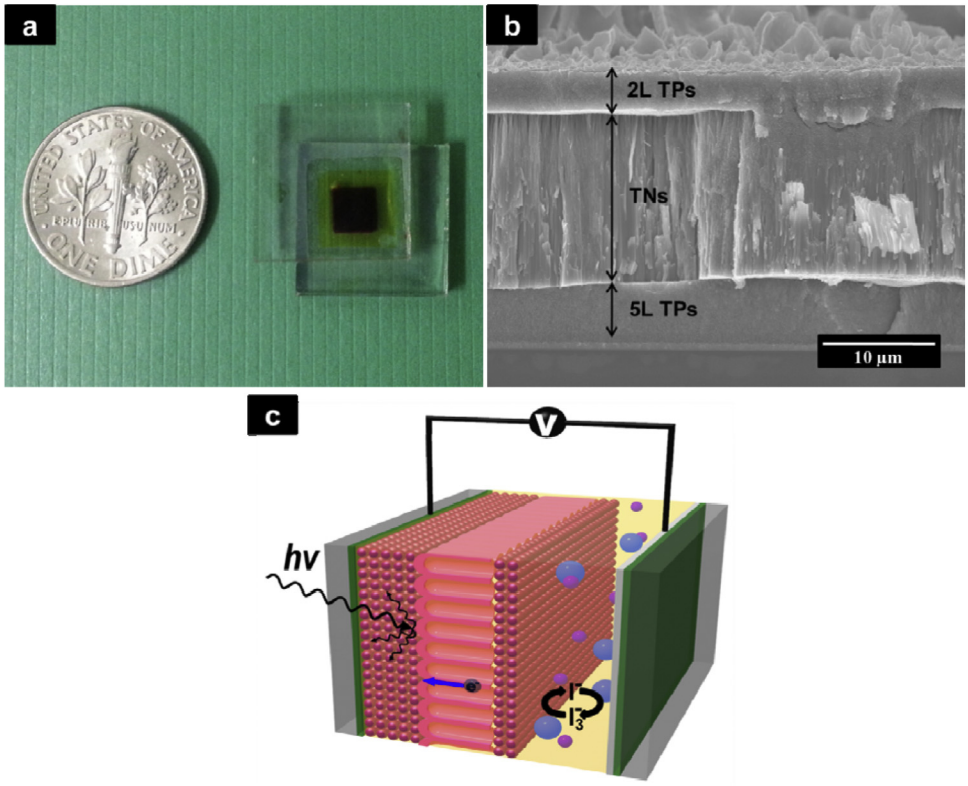

Fig. 4. (a) Photograph of a DSSC fabricated with an E-type photoanode. (b) Cross-sectional SEM image of the E-type photoanode. (c) Across-sectional schematic of the cell fabricated with an E-type photoanode.

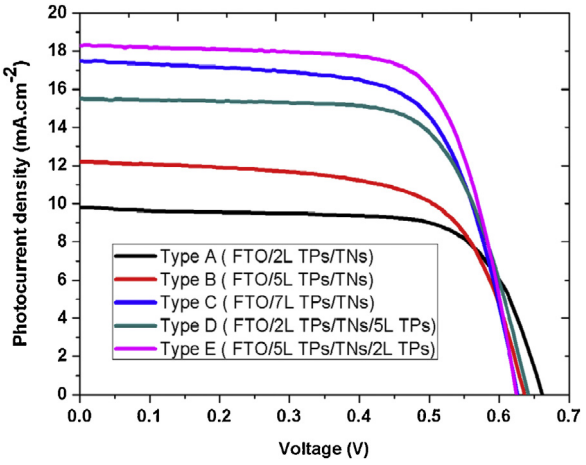

Fig. 5. J-V curves of the various DSSCs fabricated through the layer-by-layer assembly of TNs and TPs.

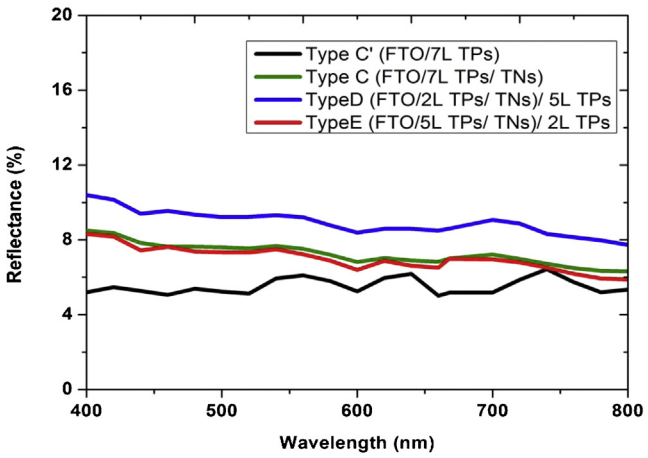

Fig. 6. UV-Vis measurements of the various DSSCs fabricated through the layer-by-layer assembly of TNs and TPs.

anode structures, vertically aligned and continuous TNs have fewer interfaces, which facilitate electron transport with a low chance of charge recombination and further enhances the PCE. The D-type cell has the same volume of photo sensitive materials as the E-type cell, but the stacking sequence of D is the reverse of E; the two layers of TPs are placed on the FTO glass, not on top of the TNs. The thinner layer of TPs does not give sufficient space to create electrons after the incident photons are scattered. Therefore, compared to the E-type cell, the D-type photoanode's PCE (6.5%) is approximately 13% lower. These results are comparable to the other works in references [30–32], which were very diverse from about 4 to 9 % with different conditions.

The reflectance of the C-, D-, and E-type photoanodes was measured to verify their light-scattering capabilities, with the results presented in Fig. 6. For comparison purposes, the reflectance data of a photoanode with only TP layers is also presented in Fig. 6 (labeled type C′). As shown in the graph, even though the type C′photoanode absorbed the most light, its PCE (see Table S1) is much lower than the type C photoanode, with the additional layer of TNs increasing its reflectance. Of the samples tested, the type D photoanode (FTO/2 layers (L) of TPs/TNs/5L TPs) has the highest reflectance over 400 to 800 nm, which suggests that incident light is mostly scattered by the TN layer. As a result, some of the light cannot be transmitted through the TNs and is reflected, and therefore, reduces the photoelectron generation compared to the other two photoanodes, which results in the

lower PCE of the D-type cell (6.5%). However, when TNs are placed on top of sufficiently thick TP layers, which might be more than 5 μm thick (i.e., types C and E), the incident light, including short wavelength light, is first absorbed by the TPs and then scattered by the TNs, which can generate more electrons. The long wavelength light can penetrate further, and the generated electrons are more easily transported by the TNs, which enhances the resulting PCE.

EIS was performed to investigate the kinetics of the charge transfer and recombination processes in the DSSCs. Fig. 7(a) shows the Nyquist plots of the obtained impedance data for the C-, D-, and E-type DSSCs under AM 1.5 illumination at an applied bias of V_{oc}. The equivalent circuit used to fit the experimental data for the TP/TN-based DSSCs is presented in the inset of Fig. 7(a). Upon changing the conditions, the resistances (R_s,R_1, and R_2) also changed, with Table 2 showing the parameters of the fit extracted from the Nyquist plots. The series resistance, R_s, is caused by the sheet resistance of the FTO glass, current collector contacts, etc [41]. This resistance corresponds to the value on the x-axis where the first semicircle begins [41–42]. The values of R_s are similar, which indicates that the $TiOCl_2$ treatment and TPs/TNs might have little effect on R_s [42]. The resistance R_1 is thought to be the sum of the interfacial resistances of the FTO/TiO_2 and Pt/electrolyte solution [41–42]. Therefore, because the same platinized

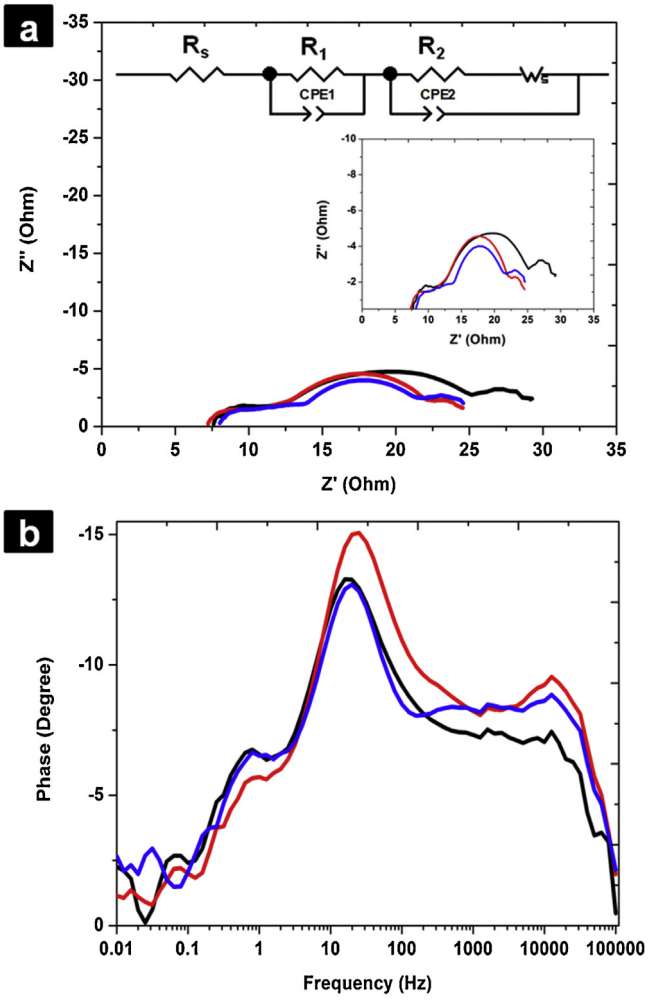

Fig. 7. Nyquist plots (a) and Bode plots (b) of the electrochemical impedance spectroscopy performed on the various DSSCs fabricated through the layer-by-layer assembly of TNs and TPs. Black, red, and blue lines are the results of 'Type C', 'Type D', and 'Type E', respectively. The y-axis rescaled Nyquist plots are added in Fig. 7(a). (For interpretation of the references to colour in this figure legend, the reader is referred to the web version of this article.)

Table 2
The photoelectron transport properties of the DSSCs fabricated with different photoanodes[b].

Type	Sample	$R_s(\Omega)$	$R_1(\Omega)$	$R_2(\Omega)$	τ(ms)
Type C	FTO/7L TPs/TNs	7.44 ± 0.08	3.96 ± 0.23	14.5 ± 0.63	7.98
Type D	FTO/2L TPs/TNs/5L TPs	6.59 ± 0.12	5.98 ± 0.41	9.54 ± 0.67	6.33
Type E	FTO/5L TPs/TNs/2L TPs	7.17 ± 0.07	7.66 ± 0.19	5.51 ± 0.47	7.98

[b] R_s = sheet resistance, R_1 = interfacial resistance, R_2 = charge transfer resistance, τ= electron lifetime

conducting glass substrate was used as the counter electrodes for all DSSCs devices, the value of R_1 might be affected by the different FTO/TP/TN interfacial properties. The C-type DSSC (FTO/7L TPs/TNs) has the smallest value of R_1 of the three types (C, D, and E) of DSSCs tested, which suggests that electron extraction occurs between the TPs and glass. The photocurrent density is affected by the charge collection efficiency, which is related to the electron lifetime. The resistance R_2 is thought to be the sum of the charge transfer resistances of the TP/TN layers and the dye-adsorbed TP/TN layers/electrolyte interfaces [41]. Fig. 7(b) shows the Bode plots of the EIS measurements for the three different photoanodes. The lifetime of photoelectrons (τ) in a photoanode can be calculated according to the following equation [42]:

$$\tau = \frac{1}{\omega_{peak}} = \frac{1}{2\pi f_{peak}} \quad (1)$$

where ω_{peak} and f_{peak} are the peak angular and oscillation frequencies, respectively, of the impedance semicircle in the medium-frequency region. From the Bode plots, the values of fpeak for the C- (FTO/7L TPs/TNs), D- (FTO/2L TPs/TNs/5L TPs), and E-type (FTO/5L TPs/TNs/2L TPs) photoanodes are 19.95, 25.12, and 19.95 Hz, respectively, and the corresponding values of τ are 7.98, 6.33, and 7.98ms, respectively. Therefore, compared to the other photoanodes, the lifetime of photo generated electrons in the D-type cell is lower. Interestingly, the C-type cell has similar optical properties, electron lifetime, and a slightly lower conversion efficiency compared to the E-type cell, but the interfacial resistance and charge transfer resistance of these two structures are quite different. One might suggest that when the 2 TP layers are stacked on the TNs, it could cause defects between the TP/TN interfaces, but these 2 TPs layers effectively contribute to the charge transfer process. Therefore, by using hybrid photoanode structures, it is concluded that the optimal stacking process can effectively increase the PCE.

4. Conclusions

We have successfully fabricated highly ordered, freestanding, TN membranes with a two-step anodization and detaching process. With heat treatment at 500°C for 2 h, amorphous as-grown TNs were transformed to anatase crystal structure analyzed by XRD. We have successfully fabricated hybrid-structured photoanodes with the crystalline TN membranes and TPs. The TN membrane was placed on or between TP layers to generate such hybrid structures; we presumed that the TN membrane could increase the conversion of photonenergy. The properties of solar cell were characterized by solar simulator and EIS simulations. The hybrid photoanodes exhibited enhanced solar cell performances, with higher J_{sc}(18.32 mA·cm−2) and PCE (7.47%) values. This improvement was the result of increased light scattering, which prolonged the electron lifetime, and efficient charge transfer through the highly ordered TNs. It is expected that hybrid photoanodes can be extended to other composite films to improve

their characteristics to a similar degree and further enhance the efficiency of DSSCs.

Acknowledgments

This research was co-supported by 1) the Basic Science Research Program, through the National Research Foundation of Korea (NRF), which was funded by the Ministry of Education (NRF-2010-0025175), and by 2) the Civil & Military Technology Cooperation Program, through the National Research Foundation of Korea (NRF), which was funded by the Ministry of Science, ICT, & Future Planning (No. 2013M3C1A9055407).

Appendix A. Supplementary data

Supplementary data associated with this article can be found, in the online version, at http://dx.doi.org/10.1016/j.electacta.2015.05.141.

References

[1] B. O'Regan, M. Gratzel, A low-cost high- efficency solar cell based on dye sensitized colloidal TiO_2 films, Nature 353 (1991) 737.
[2] J. Burschka, N. Pellet, S.-J. Moon, R. Humphry-Baker, P. Gao, M.K. Nazeeruddin, M. Gratzel, Sequential deposition as a route to high-performance perovskite-sensitized solar cells, Nature 499 (2013) 316.
[3] M.A. Green, et al., Solar cell efficiency tables (version 42), Progress in Photovoltaics: Research and Applications 21 (2013) 827.
[4] H.M. Cheng, W.H. Chiu, C.H. Lee, S.Y. Tsai, W.F. Hsieh, Formation of branched ZnO nanowires from solvothermal method and dye-sensitized solar cells applications, J. Phys. Chem. C 112 (2008) 16359.
[5] B. Liu, E.S. Aydil, Growth of oriented single-crystalline rutile TiO_2 nanorods on transparent conducting substrates for dye-sensitized solar cells, J. Am. Chem. Soc. 131 (2009) 3985.
[6] P. Roy, S. Berger, P. Schmuki, TiO_2 nanotubes: synthesis and applications, Angew. Chem., Int. Ed 50 (2011) 2904.
[7] P. Roy, D. Kim, K. Lee, E. Spiecker, P. Schmuki, TiO_2 nanotubes and their application in dye-sensitized solar cells, Nanoscale 2 (2010) 45.
[8] J. Wang, Z. Lin, Freestanding TiO_2 nanotube arrays with ultrahigh aspect ratio via electrochemical anodization, Chem. Mater. 20 (2008) 1257.
[9] J. Wang, Z. Lin, Anodic formation of ordered TiO_2 nanotube arrays: effects of electrolyte temperature and anodization potential, J. Phys. Chem. C 113 (2009) 4026.
[10] J. Wang, L. Zhao, V.S.Y. Lin, Z. Lin, Formation of various TiO_2 nanostructures from electrochemically anodized titanium, J. Mater. Chem. 19 (2009) 3682–3687.
[11] S. Yoriya, C.A. Grimes, Self-assembled TiO_2 nanotube arrays by anodization of titanium in diethylene glycol: approach to extended pore widening, Langmuir 26 (2009) 417.
[12] N. Liu, K. Lee, P. Schmuki, Small diameter TiO_2 nanotubes vs. nanopores in dye sensitized solar cells, Electrochem. Commun. 15 (2012) 1.
[13] J. Park, S. Bauer, K.A. Schlegel, F.W. Neukam, K. von der Mark, P. Schmuki, TiO_2 nanotube surfaces: 15 nm—an optimal length scale of surface topography for cell adhesion and differentiation, Small 5 (2009) 666.
[14] C.C. Chen, H.W. Chung, C.H. Chen, H.P. Lu, C.M. Lan, S.F. Chen, L. Luo, C.S. Hung, E.W.G. Diau, Fabrication and characterization of anodic titanium oxide nanotube arrays of controlled length for highly efficient dye-sensitized solar cells, J. Phys. Chem. C 112 (2008) 19151.
[15] P. Roy, D. Kim, I. Paramasivam, P. Schmuki, Improved efficiency of TiO_2 nanotubes in dye sensitized solar cells by decoration with TiO_2 nanoparticles, Electrochem. Commun. 11 (2009) 1001.
[16] Y. Alivov, Z.Y. Fan, Efficiency of dye sensitized solar cells based on TiO_2 nanotubes filled with nanoparticles, Appl. Phys. Lett 95 (2009) 063504.
[17] C. Rho, J.S. Suh, Filling TiO_2 nanoparticles in the channels of TiO_2 nanotube membranes to enhance the efficiency of dye-sensitized solar cells, Chem. Phys. Lett. 513 (2011) 108.
[18] S. Wang, J. Zhang, S. Chen, H. Yang, Y. Lin, X. Xiao, X. Zhou, X. Li, Conversion enhancement of flexible dye-sensitized solar cells based on TiO_2 nanotube arrays with TiO_2 nanoparticles by electrophoretic deposition, Electrochim. Acta 56 (2011) 6184.
[19] M. Ye, X. Xin, C. Lin, Z. Lin, High efficiency dye-sensitized solar cells based on hierarchically structured nanotubes, Nano Lett. 11 (2011) 3214–3220.
[20] C.C. Xuan Pan, K. Zhu, Z. Fan, TiO_2 nanotubes infiltrated with nanoparticles for dye sensitized solar cells, Nanotechnology 22 (2011) 5088.
[21] M.G. Kang, N.-G. Park, K.S. Ryu, S.H. Chang, K.-J. Kim, A 4. 2% efficient flexible dye-sensitized TiO_2 solar cells using stainless steel substrate, Sol. Energy Mater. Sol. Cells 90 (2006) 574.
[22] G.K. Mor, O.K. Varghese, M. Paulose, C.A. Grimes, Transparent highly ordered TiO_2 nanotube arrays via anodization of titanium thin films, Adv. Funct. Mater. 15 (2005) 1291.
[23] G.K. Mor, K. Shankar, M. Paulose, O.K. Varghese, C.A. Grimes, Use of highly-ordered TiO_2 nanotube arrays in dye-sensitized solar cells, Nano Lett. 6 (2005) 215.
[24] B.Y. Yu, A. Tsai, S.P. Tsai, K.T. Wong, Y. Yang, C.W. Chu, J.J. Shyue, Efficient inverted solar cells using TiO_2 nanotube arrays, Nanotechnology 19 (2008) 255202.
[25] M. Paulose, K. Shankar, O.K. Varghese, G.K. Mor, C.A. Grimes, Application of highly-ordered TiO2 nanotube-arrays in heterojunction dye-sensitized solar cells, J. Phys. D: Appl. Phys. 39 (2006) 2498.
[26] H. Zheng, A.Z. Sadek, M. Breedon, D. Yao, K. Latham, J. d. Plessis, K. Kalantar-Zadeh, Fast formation of thick and transparent titania nanotubular films from sputtered Ti, Electrochem. Commun. 11 (2009) 1308.
[27] O.K. Varghese, M. Paulose, C.A. Grimes, Long vertically aligned titania nanotubes on transparent conducting oxide for highly efficient solar cells, Nat. Nanotechnol. 4 (2009) 592.
[28] C.J. Lin, W.Y. Yu, S.H. Chien, Transparent electrodes of ordered opened-end TiO_2-nanotube arrays for highly efficient dye-sensitized solar cells, J. Mater. Chem. 20 (2010) 1073.
[29] Q. Chen, D. Xu, Large-scale, noncurling, and free-standing crystallized TiO_2 nanotube arrays for dye-sensitized solar cells, J. Phys. Chem. C 113 (2009) 6310.
[30] Q. Zheng, H. Kang, J. Yun, J. Lee, J.H. Park, S. Baik, Hierarchical construction of self-standing anodized titania nanotube arrays and nanoparticles for efficient and cost-effective front-illuminated dye-sensitized solar cells, ACS Nano 5 (2011) 5088.
[31] H.G. Yun, J.H. Park, B.S. Bae, M.G. Kang, Dye-sensitized solar cells with TiO_2 nano-particles on TiO_2 nano-tube-grown Ti substrates, J. Mater. Chem. 21 (2011) 3558.
[32] X. Xin, J. Wang, W. Han, M. Ye, Z. Lin, Dye-sensitized solar cells based on a nanoparticle/nanotube bilayer structure and their equivalent circuit analysis, Nanoscale 4 (2012) 964.
[33] S. Li, G. Zhang, D. Guo, L. Yu, W. Zhang, Anodization fabrication of highly ordered TiO_2 nanotubes, J. Phys. Chem. C 113 (2009) 12759.
[34] C.T. Yip, M. Guo, H. Huang, L. Zhou, Y. Wang, C. Huang, Open-ended TiO_2 nanotubes formed by two-step anodization and their application in dye-sensitized solar cells, Nanoscale 4 (2012) 448.
[35] J.Y. Ahn, J.H. Kim, K.J. Moon, S.D. Park, S.H. Kim, Synergistic effects of the aspect ratio of TiO_2 nanowires and multi-walled carbon nanotube embedment for enhancing photovoltaic performance of dye-sensitized solar cells, Nanoscale 5 (2013) 6842.
[36] P. Joshi, L. Zhang, D. Davoux, Z. Zhu, D. Galipeau, H. Fong, Q. Qiao, Composite of TiO_2 nanofibers and nanoparticles for dye-sensitized solar cells with significantly improved efficiency, Energy Environ. Sci. 3 (2010) 1507.
[37] P. Roy, S.P. Albu, P. Schmuki, TiO_2 nanotubes in dye-sensitized solar cells: higher efficiencies by well-defined tube tops, Electrochem. Commun. 12 (2010) 949.
[38] E. Ghadiri, N. Taghavinia, S.M. Zakeeruddin, M. Gratzel, J.E. Moser, Enhanced electron collection efficiency in dye-sensitized solar cells based on nanostructured TiO_2 hollow fibers, Nano Lett. 10 (2010) 1632.
[39] S. Ito, T. Takeuchi, T. Katayama, M. Sugiyama, M. Matsuda, T. Kitamura, Y. Wada, S. Yanagida, Conductive and transparent multilayer films for low-temperature-sintered mesoporous TiO_2 electrodes of dye-sensitized solar cells, Chem. Mater 15 (2003) 2824.
[40] C. Rho, J.-H. Min, J.S. Suh, Barrier layer effect on the electron transport of the dye-sensitized solar cells based on TiO_2 nanotube arrays, J. Phys. Chem. C 116 (2012) 7213.
[41] F. Fabregat-Santiago, J. Bisquert, E. Palomares, L. Otero, D. Kuang, S.M. Zakeeruddin, M. Grätzel, Correlation between photovoltaic performance and impedance spectroscopy of dye-sensitized solar cells based on ionic liquids, J. Phys. Chem. C 111 (2007) 6550.
[42] R. Kern, R. Sastrawan, J. Ferber, R. Stangl, J. Luther, Modeling and interpretation of electrical impedance spectra of dye solar cells operated under open-circuit conditions, Electrochim. Acta 47 (2002) 4213.